Supplementary Information

Quantum teleportation of a photon via absorption and emission for quantum repeater nodes

Raustin Reyes[1], Yuhei Sekiguchi[2], Daisuke Ito[1], Taichi Fujiwara[1], Kansei Watanabe[1], Toshiharu Makino[2,3], Hiromitsu Kato[2,3], Hideo Kosaka[1,2*]

[1]Department of Physics, Graduate School of Engineering Science, Yokohama National University, 79-5, Tokiwadai, Hodogaya, Yokohama, 240-8501, Japan.
[2]Quantum Information Research Center, Institute of Advanced Sciences, Yokohama National University, 79-5, Tokiwadai, Hodogaya, Yokohama, 240-8501, Japan.
[3]Advanced Power Electronics Research Center, National Institute of Advanced Industrial Science and Technology, 1-1-1, Umezono, Tsukuba, Ibaraki, 305-8568, Japan.

*Corresponding author(s). E-mail(s): kosaka-hideo-yp@ynu.ac.jp;

1 Supplementary Note 1. GRAPE pulse

To enhance the fidelity of quantum operations, we explore optimized waveforms using the GRAPE algorithm [1]. In this study, we optimize the microwave pulses employed for generating spin entanglement between electron and nitrogen spins (Fig. 1a) and for BSM (Fig. 1b). The waveform is produced through intensity modulation, which not only improves operational fidelity even at lower Rabi frequencies but also optimizes the waveform to prevent population transitions to the entangle states $|\Psi^{\pm}\rangle_{\mathrm{S,N}}$.

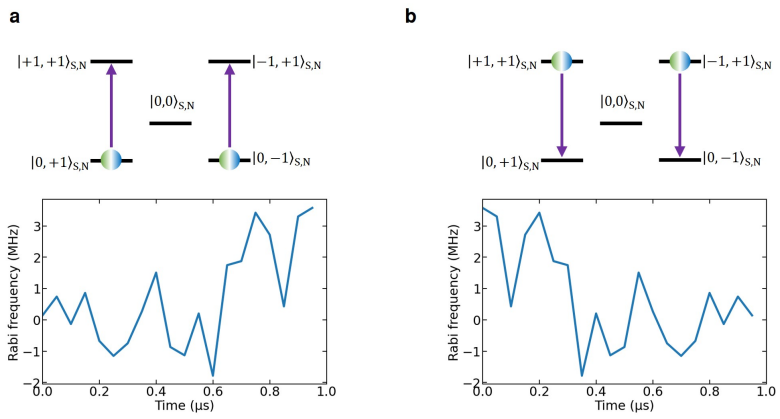

Fig. 1 Microwave pulses generated by the GRAPE algorithm. In this study, MW pulses for **a**, electron–nitrogen spin entanglement generation and **b**, Bell state measurement are optimized by modulating their intensity using the GRAPE algorithm.

2 Supplementary Note 2. Quantum State Tomography (QST) of electron–nitrogen spin entanglement

In QST [2], for each spin, we measure the expectation values in the geometric qubit space for $\sigma_0(\sigma_x, \sigma_y, \sigma_z) \otimes \sigma_0(\sigma_x, \sigma_y, \sigma_z)$ and use the results to estimate the density matrix. This density matrix, ρ_{exp}, is given by:

$$\rho_{\text{exp}} = \frac{1}{2^2} \sum_{i,j=0}^{3} r_i r_j \sigma_i \sigma_j, \tag{1}$$

Here, $r_0 = 1$ and $\sigma_0 = I$ represent the identity operator for a single qubit, with $\sigma_1 = \sigma_x, \sigma_2 = \sigma_y$, and $\sigma_3 = \sigma_z$. Additionally, $r_i r_j$ represents the experimentally obtained expectation values of $\sigma_i \sigma_j$, represented by $\langle \sigma_i \sigma_j \rangle = \text{Tr}[\sigma_i \sigma_j \rho_{\text{exp}}]$. The fidelity of the entanglement is evaluated by taking the trace inner product $\text{Tr}[\rho_{\text{ideal}} \rho_{\text{exp}}]$ between the ideal entangled density operator ρ_{ideal} and the experimentally obtained density matrix ρ_{exp}.

3 Supplementary Note 3. Experimental sequence

The polarization state transfer demonstration discussed in the main text is implemented using Keysight's AWG (arbitrary waveform generator, M3202A) in sequence mode along with a custom-built FPGA (field programmable gate array). The FPGA controls the trigger signals to the AWG and pulse signals to the AOM (acousto-optic modulator), while simultaneously monitoring the signals generated by photon detection via the APD (avalanche photo diode). The demonstration is designed as shown

in Fig. 2.

(i) Charge state check and nitrogen spin initialization

Upon receiving the start command from the FPGA, the charge state check of the NV center and the nitrogen spin initialization are performed first. We use negatively charged NV center (NV^-) in this study. At the beginning of the sequence, the NV charge state is initialized by green laser irradiation at 515 nm. In this initialization process, the NV may occasionally initialize to the neutrally charged state, NV^0, with a certain probability; since the resonance wavelength of NV0 is 575 nm [3], it is distinguished by irradiating laser light resonant with NV^- and observing whether photon detection occurs. The photon count distribution obtained during this charge state check is discussed later. After completing the charge state check sequence, the system proceeds to the nitrogen spin initialization sequence. Here, the electron spin state is first initialized to $|0\rangle_{\mathrm{S}}$ by irradiating laser light resonant with $|E_{12}\rangle$. After initializing the electron spin, we apply microwaves (MW) to induce a transition in the electron spin state from $|0,0\rangle_{\mathrm{S,N}}$ to $|\pm1,0\rangle_{\mathrm{S,N}}$. The frequency of this MW is set to match the zero-field splitting of the electron spin, $D_0/2\pi = 2.88$ GHz. To further enhance the fidelity of the electron spin transitions, the demonstration applies MW optimized by the GRAPE algorithm. Following the electron spin transition, we apply radio waves (RF), which are resonant with the nitrogen spin quadrupole splitting, $Q/2\pi = 4.945$ MHz, to induce a transition in the nitrogen spin from $|0,+\rangle_{\mathrm{S,N}}$ to $|0,0\rangle_{\mathrm{S,N}}$. Since the nitrogen spin forms a three-level Λ-type structure, a single transition does not polarize the entire population into $|0,0\rangle_{\mathrm{S,N}}$, so RF is applied again with orthogonal polarization to induce a transition from $|0,-\rangle_{\mathrm{S,N}}$ to $|0,0\rangle_{\mathrm{S,N}}$. Finally, after reinitializing the electron spin to $|0\rangle_{\mathrm{S}}$, a linearly polarized RF wave is applied to set the nitrogen spin to $|+\rangle_{\mathrm{N}}$.

(ii) Photon absorption and emission

In the photon absorption and emission stages, to improve the repetition rate, photon absorption and emission are attempted without reinitializing the electron and nitrogen spin states, even if photon detection fails. Due to interactions between the electron spin and surrounding carbon isotope nuclear spins, the coherence of the electron–nitrogen spin entanglement gradually decreases, so dynamical decoupling sequence is employed to suppress this decoherence. For each cycle of dynamical decoupling, an incident photon is irradiated 10 times within the decoupling pulses. To maintain the fidelity of the electron–nitrogen spin entanglement, the maximum repetition count for this stage is set to 200. As with the charge state check, this stage proceeds to the next stage only if photon detection occurs.

(iii) Bell state measurement

Since the BSM used in this study is destructive, this stage performs a single readout of the electron and nitrogen spin states with single laser irradiation. In this study, the BSM is conducted between the electron and nitrogen spins in the $|\Phi^+\rangle_{\mathrm{S,N}}$ and $|\Phi^-\rangle_{\mathrm{S,N}}$ basis by orthogonally polarized RF. The sequence first transitions the nitrogen spin state to the electron spin $|0\rangle_{\mathrm{S}}$ via RF irradiation. Then, the states that could not be transferred, $|0,+1\rangle_{\mathrm{S,N}}$ and $|0,-1\rangle_{\mathrm{S,N}}$, are transitioned to $|+1,+1\rangle_{\mathrm{S,N}}$ and $|-1,-1\rangle_{\mathrm{S,N}}$ respectively, so that only the $|0,0\rangle_{\mathrm{S,N}}$ state is read out. For the readout, the $|E_x\rangle$

state, which preserves the electron spin state, is used, and detected photon counts are recorded by the FPGA.

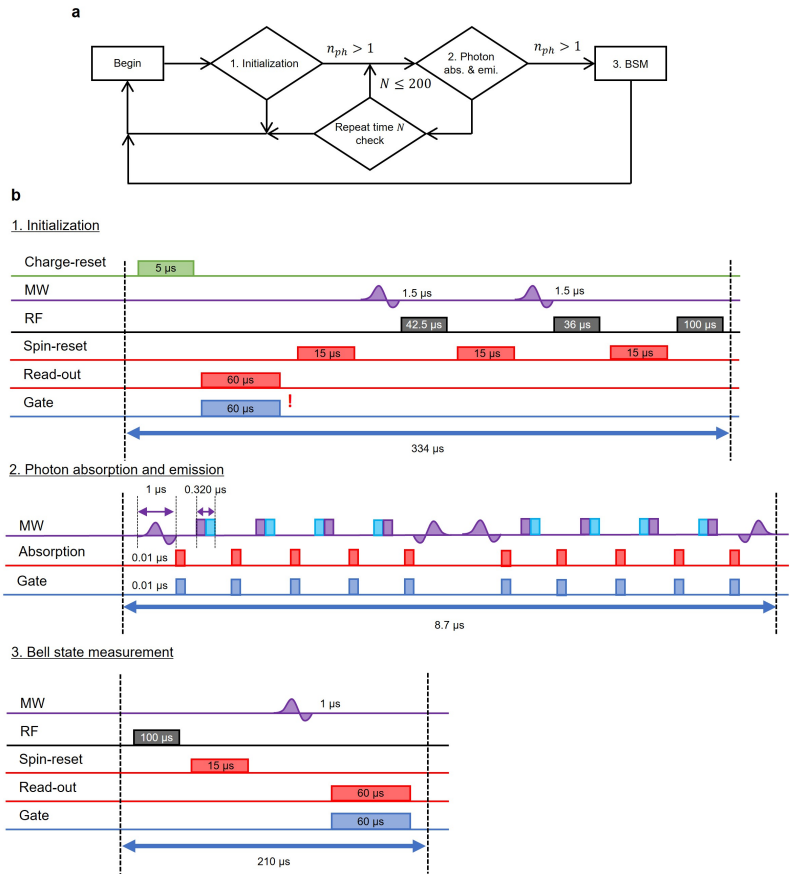

Fig. 2 Pulse sequence for the polarization state transfer demonstration. a, Flowchart of the experimental sequence. In the charge state check and photon absorption and emission stages, the demonstration progresses to the next stage only when photon detection occurs. In the photon absorption and emission stages, the maximum repetition count is set to 200 to maintain the electron–nitrogen spin entanglement fidelity; if this limit is exceeded, the sequence returns to the initial stage. **b**, Experimental sequence for each stage. The master clock is managed by the FPGA, which sends signals with preset timing and duration to control the pulsing of laser light, microwaves, and radio waves output.

4 Supplementary Note 4. Transfer rate estimation

Here, an estimate from other preliminary demonstrations is made for the transfer rate obtained in this demonstration. To enhance the photon absorption and collection efficiencies, a solid immersion lens is fabricated on the diamond surface [4, 5]. The experimental transfer rate is calculated based on the photon counts obtained in the

final BSM stage. In the photon absorption stage, once photon absorption occurs, the APD detects emission from the NV, allowing the demonstration to proceed to the next BSM stage. The probability of this transition, as shown in Table 1, is approximately $\eta_{\mathrm{abs}}\eta_{\mathrm{emi}} \approx 2 \times 10^{-6}$. Given the extremely low probability of photon acquisition in the entangled absorption and emission stages, most of the experimental time is spent on initialization and these stages. The transfer rate r is estimated from this probability, the repetition count N_{DD} of the photon absorption and emission stages, the number of incident photons N_{inc} per repetition, and the time t required for the initialization, photon absorption and emission stages. The transfer rate in the main text is defined by excluding the probability η_{C} that the NV center is in the NV^- charge state during the charge state check. If the acquired photon count in the BSM stage is n_{acq}, the acquisition time is T_{acq}, and the average photon count for spin state readout is n_{RO}, then the transfer rate is given by $r = n_{\mathrm{acq}}/(\eta_{\mathrm{C}} T_{\mathrm{acq}} n_{\mathrm{RO}})$. Details regarding η_{C} and n_{RO} are given later.

Additionally, we discuss losses not accounted for in the main text. In this study, a polarizer (THORLABS, LPVISC100-MP2) is used to measure photon polarization, with a transmission rate of approximately 75%. Furthermore, the APD (Laser Components, COUNT-10C) used for photon detection also impacts the transfer rate, with a detection efficiency of 75%. By accounting for these losses, the transfer rate can be expected to improve by approximately 1.78 times. Additionally, while we measure the charge state of the NV in this study to enhance the transfer rate, experimental efficiency could be further improved by introducing resonance check measurements, as in previous studies [6]. The Fourier-limited linewidth of the NV is approximately 20 MHz, whereas the linewidth after charge state measurement in this demonstration is about 40 MHz. Thus, introducing the resonance check measurements could potentially increase efficiency by a factor of about 2. Consequently, although the transfer rate achieved in this demonstration with an average of 0.1 incident photons is approximately 0.2 Hz, these improvements could increase the transfer rate to around 0.7 Hz.

Table 1 Parameters related to transfer rate.

Content	Value	Explanation
η_{abs}	4.1×10^{-4}	absorption efficiency
η_{emi}	5.2×10^{-3}	emission efficiency
n	0.1	average number of incident photons
N_{DD}	200	number of repetitions in photon absorption and emission trial
N_{inc}	10	number of pulses per cycle
t (s)	2.034×10^{-3}	initialization and photon absorption and emission trial time
$r = n\eta_{\mathrm{abs}}\eta_{\mathrm{emi}}N_{\mathrm{rep}}N_{\mathrm{inc}}/t$ (Hz)	0.21	estimated transfer rate

5 Supplementary Note 5. Decreasing the transfer fidelity on the average number of incident photons

The process in which the NV center absorbs and then emits a photon is probabilistic, and some experimental outcomes show cases where absorption occurs but emission detection fails. In such cases, after the initial absorption event, the electron spin transitions into a mixed state. If photon absorption occurs during this mixed state, it results in a degradation of the fidelity of electron–nitrogen spin entanglement. Here, we discuss the simulation of the dependence of fidelity on the mean number of incident photons, as shown in Fig. 3b. To simulate the above situation, we use the absorption efficiency η_{abs}, emission efficiency η_{emi}, and average number of incident photons n, as presented in Table 1. The probability of detecting a photon emitted after an NV center absorbs a photon is given by $\eta_{\mathrm{det}}(n) = n\eta_{\mathrm{abs}}\eta_{\mathrm{emi}}$. Considering the event where photon detection occurs on the N-th attempt, the probability that no photon absorption has occurred up to the $(N-1)$-th attempt is $(1-n\eta_{\mathrm{abs}})^{N-1}$. On the other hand, the complementary event $1-(1-n\eta_{\mathrm{abs}})^{N-1}$ implies that photon absorption has occurred at least once until the $(N-1)$-th attempt, leading to a fidelity of 0.5 for the entanglement. Here, let F_{once} denote the entanglement fidelity when only a single absorption event occurs. The fidelity $F(n)$ at an average number of incident photons n is then expressed by weighting with the probability $(1-\eta_{\mathrm{det}}(n))^{N-1}\eta_{\mathrm{det}}(n)$, representing photon detection occurring on the N-th attempt,

$$F(n) = \frac{\sum_{N=1}^{N_{\mathrm{DD}}} \left[(1-\eta_{\mathrm{det}}(n))^{N-1} \times \left\{(1-n\eta_{\mathrm{abs}})^{N-1}F_{\mathrm{once}} + (1-(1-n\eta_{\mathrm{abs}})^{N-1})0.5\right\}\right]}{\sum_{N=1}^{N_{\mathrm{DD}}}(1-\eta_{\mathrm{det}}(n))^{N-1}\eta_{\mathrm{det}}(n)}. \tag{2}$$

6 Supplementary Note 6. Photon count distribution during charge check and Bell state measurement

Here, we discuss the probability of charge initialization and the photon count distribution for spin state readout, both of which are relevant to calculating the transfer rate. In this study, to improve efficiency, events in which the NV charge state is neutral are excluded when entangled absorption and BSM are performed. The photon count obtained during the BSM depends on the measurement basis of the emitted photons, as the polarization of $|E_x\rangle$ used for readout is fixed. Here, we describe the photon count distribution during the BSM, preparing the electron and nitrogen spins in the entangled state $|\Phi^+\rangle_{\mathrm{S,N}}$ and showing the photon count distribution when read out in the Bell basis of $|\Phi^+\rangle_{\mathrm{S,N}}$ and $|\Phi^-\rangle_{\mathrm{S,N}}$. Fig. 3 shows the photon count distributions: a (d) shows the distribution when the polarizer is set to $|+\rangle_{\mathrm{P_{out}}}$ ($|-\rangle_{\mathrm{P_{out}}}$) during the charge check, b (e) shows the distribution in the Bell basis $|\Phi^+\rangle_{\mathrm{S,N}}$, and c (f) shows the distribution in $|\Phi^-\rangle_{\mathrm{S,N}}$. In this study, the demonstration proceeds to the next entangled absorption stage if the photon count is one or more during the charge check. Thus, the probability that the NV center is in the NV- state during the charge check is given by the complement of the event in which the photon count is zero in

the distribution. On the other hand, the average number of photons obtained during the BSM is calculated from the expectation value of the photon count distribution.

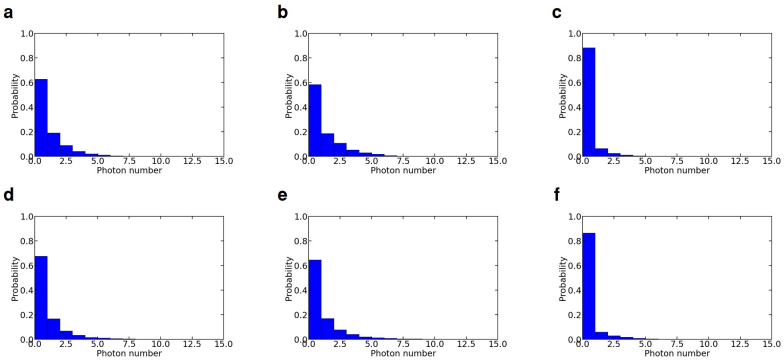

Fig. 3 Photon count distribution during charge initialization and BSM. Photon count distribution during **a**, and **d**, charge check; **b**, and **e**, $|\Phi^+\rangle_{\mathrm{S,N}}$; and **c**, and **f**, $|\Phi^-\rangle_{\mathrm{S,N}}$ BSM basis. The distributions correspond to measurements taken when the polarization of the emitted photons is set to the $|+\rangle_{\mathrm{P_{out}}}$ or $|-\rangle_{\mathrm{P_{out}}}$ basis, respectively. When the polarization of emitted photons is measured in the $|+\rangle_{\mathrm{P_{out}}}$ ($|-\rangle_{\mathrm{P_{out}}}$) basis, the probability of the NV center being in the NV^- state during the charge check is $\eta_{\mathrm{C}} = 0.381(0.295)$, and the average photon count during the BSM is $n_{\mathrm{RO}} = 1.126(1.125)$.

7 Supplementary Note 7. Quantum frequency conversion (QFC)

Here, we describe the efficiency of QFC. In the emission-absorption scheme, it is essential to use difference-frequency generation (DFG) to convert visible photons emitted by the NV (637 nm) into telecommunications wavelength photons (1550 nm) and then to use sum-frequency generation (SFG) for reverse conversion back to the visible range for reabsorption by the NV center. A nonlinear crystal is used for the QFC process. In this study, a periodically poled lithium niobate (PPLN) waveguide device is used, and QFC is performed by incident pump light at 1082 nm, corresponding to the difference between the visible and telecommunications wavelengths. The QFC efficiency is expressed as $\eta \sin^2(\sqrt{\kappa P})$, where η is the maximum conversion efficiency, P is the intensity of the incident pump light, and κ is the coupling efficiency of the pump light into the waveguide [7]. By fitting the experimental results to this expression, the conversion efficiencies are determined to be 0.502 for DFG and 0.424 for SFG (Fig. 4).

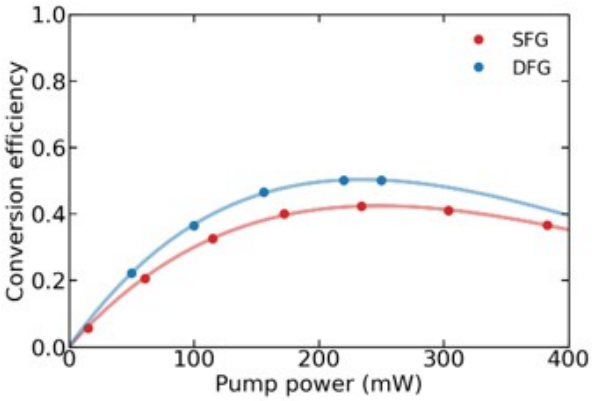

Fig. 4 Efficiency of quantum frequency conversion (QFC). The QFC system is constructed and its conversion efficiency is evaluated. In the emission-absorption scheme, conversion between the visible band (637 nm) and the telecommunications band (1550 nm) is achieved through difference-frequency generation (DFG) and sum-frequency generation (SFG). QFC is performed by directing a 1082 nm pump light , corresponding to the wavelength difference between the visible and telecommunications bands, into a periodically poled lithium niobate waveguide. By varying the intensity of the pump light in the QFC system, the conversion efficiency is measured, yielding maximum efficiencies of 0.502 for DFG and 0.424 for SFG.

References

[1] Khaneja, N., Reiss, T., Kehlet, C., Schulte-Herbrüggen, T., Glaser, S.J.: Optimal control of coupled spin dynamics: design of nmr pulse sequences by gradient ascent algorithms. Journal of magnetic resonance **172**(2), 296–305 (2005)

[2] James, D.F., Kwiat, P.G., Munro, W.J., White, A.G.: Measurement of qubits. Physical Review A **64**(5), 052312 (2001)

[3] Kurokawa, H., Wakamatsu, K., Nakazato, S., Makino, T., Kato, H., Sekiguchi, Y., Kosaka, H.: Coherent electric field control of orbital state of a neutral nitrogen-vacancy center. Nature Communications **15**(1), 4039 (2024)

[4] Hadden, J., Harrison, J., Stanley-Clarke, A.C., Marseglia, L., Ho, Y.-L., Patton, B., O'Brien, J.L., Rarity, J.: Strongly enhanced photon collection from diamond defect centers under microfabricated integrated solid immersion lenses. Applied Physics Letters **97**(24) (2010)

[5] Siyushev, P., Kaiser, F., Jacques, V., Gerhardt, I., Bischof, S., Fedder, H., Dodson, J., Markham, M., Twitchen, D., Jelezko, F., et al.: Monolithic diamond optics for single photon detection. Applied physics letters **97**(24) (2010)

[6] Humphreys, P.C., Kalb, N., Morits, J.P., Schouten, R.N., Vermeulen, R.F., Twitchen, D.J., Markham, M., Hanson, R.: Deterministic delivery of remote entanglement on a quantum network. Nature **558**(7709), 268–273 (2018)

[7] Ikuta, R., Kobayashi, T., Yasui, S., Miki, S., Yamashita, T., Terai, H., Fujiwara, M., Yamamoto, T., Koashi, M., Sasaki, M., *et al.*: Frequency down-conversion of 637 nm light to the telecommunication band for non-classical light emitted from nv centers in diamond. Optics express **22**(9), 11205–11214 (2014)